# Electronic Supplementary Information

# Performance Enhancement of Ultra-Small Core–Shell Au@AuPt Nanoparticles towards the HER and ORR by Surface Engineering

*Xinru Yue,[a] Xiang Zhang,[a] Mengmeng Zhang,[a] Wei Du,[b,*] and Haibing Xia[a,*]*

[a] State Key Laboratory of Crystal Materials, Shandong University, Jinan, 250100 P. R. China

[b] School of Environment and Material Engineering, Yantai University, Yantai 264005, P. R. China.

## 1. Experimental section

**1.1 Synthesis of pure Pt NPs and pure Au NPs.** A typical synthetic procedure of pure Pt NPs is as follows.[1] Firstly, an aqueous solution of ascorbic acid (0.5 M, 0.1 mL) was added into an aqueous solution of $K_2PtCl_4$ (5 mM, 1 mL) under stirring. Then, pure Pt NPs were generated after the heating of 10 min at 70°C until the color changed to dark gray.

A typical synthetic procedure of 6 nm Au NPs is as follows.[2] Firstly, an aqueous solution of $HAuCl_4$ (25 mM, 0.5 mL) was added into an aqueous solution of citrate (1 wt%, 2.5 mL) under stirring. Then, the as-prepared premixture was rapidly added to the boiling water (47 mL) after the stirring of 13 minutes (light green). Eventually, 6 nm Au NPs were obtained after the heating of 30 minutes.

The as-prepared Pt NPs and Au NPs were used in XPS measurements.

## 2. Characterization.

Transmission electron microscopy (TEM) images were obtained with a JEOL JEM 2100F transmission electron microscope operating at an accelerating voltage of 200kV. High-angle annular dark-field-scanning transmission electron microscopy (HAADF-STEM) and HAADF-STEM energy dispersive X-ray spectroscopy (EDS) mapping images were performed by a JEOL JEM 2100F electron microscope with a STEM unit. X-ray photoelectron spectroscopy (XPS) measurements were carried out on an ESCALAB 250 spectrometer with Al Kα X-ray radiation (1.4866 keV) for excitation. Inductively coupled plasma atomic emission spectroscopy (ICP-AES, Agilent 725) was used to obtain the elemental composition of the samples.

**3. Electrochemical measurements.**

Electrochemical measurements for the HER were performed on a CHI 660D electrochemical workstation with a conventional three-electrode system in 0.5 M $H_2SO_4$ solution at room temperature. A glassy carbon electrode (GCE, 0.07 $cm^2$) and a graphite rod were used as the working electrode and the counter electrode, respectively. An Ag/AgCl electrode was used as the reference electrode. All the measured potentials were calibrated to the reversible hydrogen electrode (RHE) by $E_{(RHE)} = E_{(Ag/AgCl)} + 0.214$ V.

A typical preparation of the RDE modified by the USCS$^{2h}$ $Au_{38.4}$@$Au_{4.1}Pt_{57.5}$-NP/C catalysts was as follows. The catalysts ink was prepared by re-dispersing the as-prepared USCS$^{2h}$ $Au_{38.4}$@$Au_{4.1}Pt_{57.5}$-NP/C powder (about 1 mg) into 1.15 ml of Milli-Q water, followed by the ultrasonication of 30 min. Then, the well-dispersed catalysts ink (8 ul) was dropped onto the clean surface of the bare RDE and dried naturally in air, followed by addition of the ethanol solution of Nafion (4 ul, 0.2wt%) and drying in air. Similarly, the RDEs modified by the USCS$^0$ Au@AuPt-NP/C catalysts and commercial Pt/C catalysts were prepared by the same procedure. The loaded Pt for USCS$^{2h}$ $Au_{38.4}$@$Au_{4.1}Pt_{57.5}$-NP/C catalysts, USCS$^0$ Au@AuPt-NP/C catalysts and commercial Pt/C catalysts on the GCEs was 4.80 $ug_{Pt}$ $cm^{-2}$, 4.82 $ug_{Pt}$ $cm^{-2}$ and 7.83 $ug_{Pt}$ $cm^{-2}$ (determined by ICP-AES), respectively.

Cyclic voltammogram (CV) measurements were tested at a scan rate of 50 mV $s^{-1}$ by cycling from −0.3 V to 0.1 V (vs. RHE) in the $N_2$-saturated 0.5 M $H_2SO_4$ solution. Linear sweep voltammetry (LSV) curves were obtained at a scan rate of 5 mV $s^{-1}$. All the LSV curves were calibrated by iR-correction. Electrochemical impedance spectroscopy (EIS) measurements

were conducted in the frequency range from 100 kHz to 0.1 Hz at the amplitude of 5 mV under the applied potential of −0.23 V (vs. RHE). The stability of USCS$^{2h}$ $Au_{38.4}$@$Au_{4.1}Pt_{57.5}$-NP/C catalysts and commercial Pt/C catalysts were tested by the accelerated durability tests (ADTs) from 0.11 to −0.05 (vs. RHE) at a scan rate of 100 mV $s^{-1}$ for 5000 cycles.

Electrochemical measurements for the ORR were performed using a CHI 601E electrochemical workstation in 0.1 M $HClO_4$ solution at room temperature. A standard three-electrode system was consisted of a saturated calomel electrode (SCE) as the reference electrode, a platinum wire as the counter electrode, and a rotating disk electrode (RDE, 0.19625 $cm^2$) as the working electrode. All the measured potentials were converted to the reversible hydrogen electrode (RHE) by the Nernst equation ($E_{RHE} = E_{SCE} + 0.0591 \times pH + 0.241$). All bare RDEs were carefully polished and washed before measurements.

The preparation of the GCEs modified by samples were prepared using the same method for the HER measurements. However, the loaded Pt for USCS$^{2h}$ $Au_{38.4}$@$Au_{4.1}Pt_{57.5}$-NP/C catalysts, USCS$^0$ Au@AuPt-NP/C catalysts and commercial Pt/C catalysts was 16.2 $ug_{Pt}$ $cm^{-2}$,16.4 $ug_{Pt}$ $cm^{-2}$ and 24.5 $ug_{Pt}$ $cm^{-2}$ (evaluated by ICP-AES), respectively.

Prior to the ORR measurement, high purity $N_2$ or $O_2$ was bubbled into the electrolyte (0.1 M $HClO_4$) for 30 min.

CV curves were measured between 0 and 1.7 V (vs. RHE) at a scan rate of 100 mV $s^{-1}$ in $N_2$-saturated 0.1 M $HClO_4$, which were employed to estimate the atomic ratios of Pt and Au on the surfaces by integrating the charge consumed for the reduction of Pt oxide (543 μC $cm^{-2}$) and the Au oxide (493 μC $cm^{-2}$), respectively. In addition, the electrochemically active surface

area (ECSA) values of these catalysts were calculated by integrating the charge obtained from the hydrogen adsorption/desorption region (0 to 0.4 V vs. RHE) after double-layer correction, assumed that 210 μC $cm^{-2}$ is the charge consumed to oxidize a hydrogen monolayer on the Pt surface.

LSV curves were recorded with a sweep rate of 10 mV $s^{-1}$ at various rotating speeds ranging from 400 to 1600 rpm in the $O_2$-saturated 0.1 M $HClO_4$ solution. The ADTs were conducted by cycling between 0.6 and 1.1 V (vs. RHE) at 100 mV $s^{-1}$ in the $O_2$-saturated 0.1 M $HClO_4$ solution for 5000 cycles. Chronoamperometric (CA) measurements of commercial Pt/C catalysts and USCS[2h] $Au_{38.4}$@$Au_{4.1}Pt_{57.5}$-NP/C catalysts were performed at 0.5 V (vs. RHE) in the $O_2$-saturated 0.1 M $HClO_4$ solution at a speed of 1600 rpm.

The electron transfer number during the ORR process was calculated by the following Koutecký-Levich equation:

$$\frac{1}{j}=\frac{1}{j_k}+\frac{1}{j_l}=\frac{1}{j_k}+\frac{1}{B\omega^{1/2}}$$

$$B = 0.62nFC_0D_0^{2/3}v^{-1/6}$$

where $j$ is the measured current density, $j_k$ is the kinetic current density and $j_l$ is the diffusion limiting current density. $\omega$ is the angular velocity ($\omega = 2\pi N$, $N$ is the linear rotation speed), $n$ is the number of transferred electrons, $F$ is the Faraday constant (96 485 C $mol^{-1}$), $C_0$ is the oxygen solubility ($1.2\times10^{-6}$ mol $cm^{-3}$), $D_0$ is the diffusivity of oxygen in 0.1 M $HClO_4$ solution ($1.9\times10^{-5}$ $cm^2$ $s^{-1}$), and $v$ is the kinetic viscosity of the electrolyte (0.01$cm^2$ $s^{-1}$).

The mass activity (MA) for HER was calculated by the following equation:

$$MA=\frac{IS}{m}$$

where I is the current, S is the area of electrode for HER (0.07 $cm^2$), m is the mass of Pt.

The turnover frequency (TOF) was obtained according to the following equation:

$$TOF = \frac{I}{2Fn}$$

where I is the current, F is the faraday constant (96485 C $mol^{-1}$), and n is the number of moles of Pt.

MA for ORR is obtained according to the following equation:

$$MA = \frac{j_k S}{m}$$

where $j_k$ is the kinetic current density, S is the area of electrode for ORR (0.19625 $cm^2$), m is the mass of Pt.

The specific activity (SA) for HER and ORR is obtained according to the following equation:

$$SA = \frac{MA \times 100}{ECSA}$$

where MA is the mass activity, ECSA is the electrochemically active surface area.

**Figure S1.** CV curves normalized by the intensity of the reduction peak of Pt oxide of USCS[0] Au@AuPt-NP/C catalysts (a) in the presence of different concentrations of $FeCl_3$ solution with a pH of 1.5 etching for 1 h: 9 mM (b), 33 mM (c), and 64 mM (d). Note that to avoid the hydrolysis of Fe(III), the pH value of the whole solution was selected as 1.5.

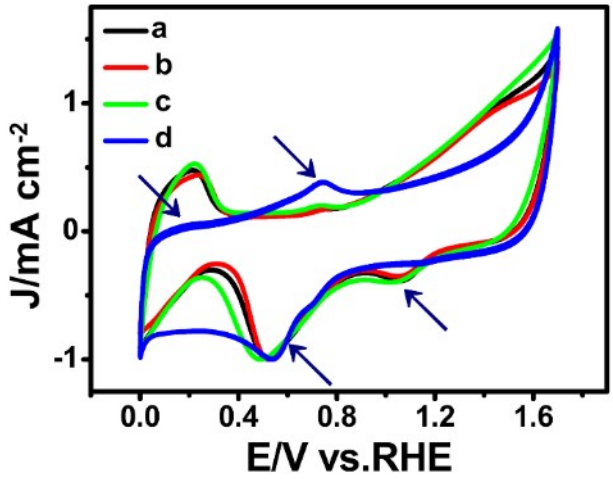


It is reasonable that the etching rate is increased with the concentration of Fe(III) ions. To limit the etching time within 1 ~3 h, the proper concentration of Fe(III) ions has to be selected. The total etching time was determined by the variation in the intensity of reduction peaks of Au oxide (around 1.1 V vs. RHE). When the concentration of Fe(III) ions is 64 mM, the reduction peak of Au oxide (around 1.1 V vs. RHE) is completely disappeared. Thus, the proper concentration of Fe(III) ions should be equal or below 33 mM.

**Figure S2.** CV curves normalized by the intensity of the reduction peak of Pt oxide of USCS[0] Au@AuPt-NP/C catalysts (a) in the presence of $FeCl_3$ solution (9 mM) with a pH of 1.5 etching for different times: 1 h (b) and 18 h (c).

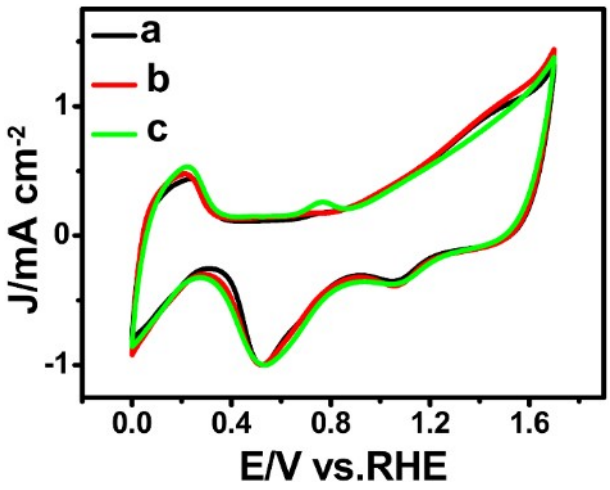


When the concentration of Fe(III) ions is 9 mM and the etching time is 1 h, there is hardly any change in the CV curves (red curve in Fig. S2). Moreover, there is only a slight change in the CV curve even the etching time is elongated to 18 h (green curve in Fig. S2). The results indicate the etching rate is too slow when the concentration of $FeCl_3$ solution is 9 mM. Thus, the proper concentration of Fe(III) ions is selected as 33 mM.

**Figure S3.** CV curve of USCS$^0$ Au@AuPt-NP/C catalysts as a sample for the determination of the surface atomic ratio of Pt and Au.

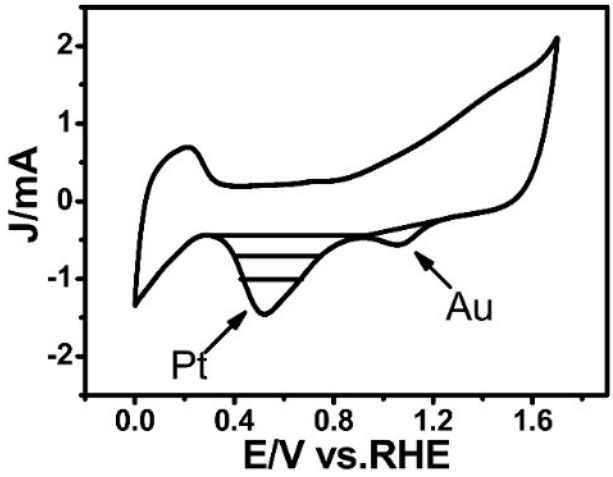


The surface atomic ratio of Pt and Au of USCS$^0$ Au@AuPt-NP/C catalysts can be calculated as follows:

$$m_{Pt} = \frac{S_{Pt}}{S_{Pt} + S_{Au}} \times 100 \quad (1)$$

$$m_{Au} = \frac{S_{Au}}{S_{Pt} + S_{Au}} \times 100 \quad (2)$$

$$S_{Pt} = \frac{Q_{Pt}(C)}{543(\mu C cm^{-2})} \quad (3)$$

$$S_{Au} = \frac{Q_{Au}(C)}{493(\mu C cm^{-2})} \quad (4)$$

$$Q_{Pt} = \frac{\int_a^b idE(mAV)}{v(mV/s)} \quad (5)$$

$$Q_{Au} = \frac{\int_c^d idE(mAV)}{v(mV/s)} \quad (6)$$

where $m_{Pt}$ and $m_{Au}$ represent the surface atomic ratio of Pt and Au, and $S_{Pt}$ and $S_{Au}$ are the surface areas covered by Pt and Au oxides, respectively. Moreover, the charge associated to the reduction of oxide species of Pt and Au are 543 μC cm$^{-2}$ and 493 μC cm$^{-2}$ respectively. Furthermore, $Q_{Pt}$ and $Q_{Au}$ are the calculated charge of the surface areas covered by Pt and Au oxides, respectively.

**Figure S4.** (A) CV curves normalized by the intensity of the reduction peak of Pt oxide and (B) LSV curves of USCS$^{mh}$ Au@AuPt-NP/C catalysts (a to d) obtained by etching of USCS Au@AuPt-NP/C catalysts in the $FeCl_3$ solution (33 mM, pH = 1.5) under different times: USCS$^{0}$ Au@AuPt-NP/C catalysts (a, black curve, 0 h), USCS$^{1h}$ Au@AuPt-NP/C catalysts (b, red curve, 1 h), USCS$^{2h}$ Au@AuPt-NP/C catalysts (c, green curve, 2 h), and USCS$^{3h}$ Au@AuPt-NP/C catalysts (d, blue curve, 3 h). (C) Histogram of their corresponding $E_{1/2}$ values. The CV curve, LSV curve and $E_{1/2}$ value of commercial Pt/C catalysts (e) were also shown for better comparison.

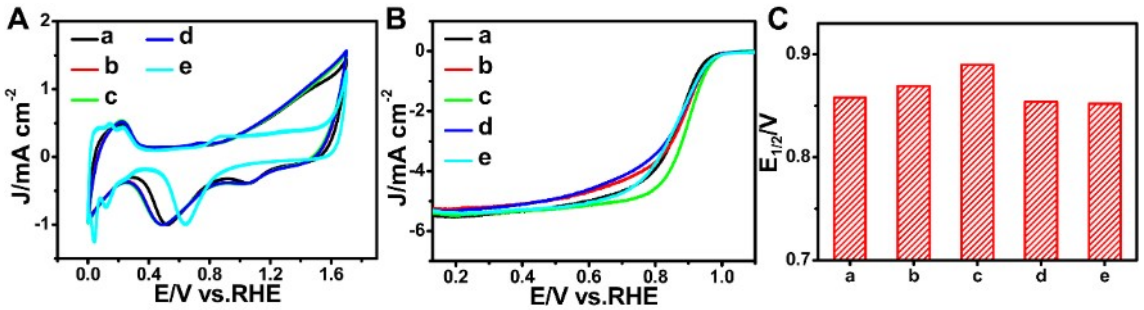

**Figure S5.** Low magnification TEM images of USCS$^0$ Au@AuPt-NP/C catalysts in the presence of $FeCl_3$ solution (33 mM) with a pH of 1.5 etching for different times: 1 h (a) and 3 h (b).

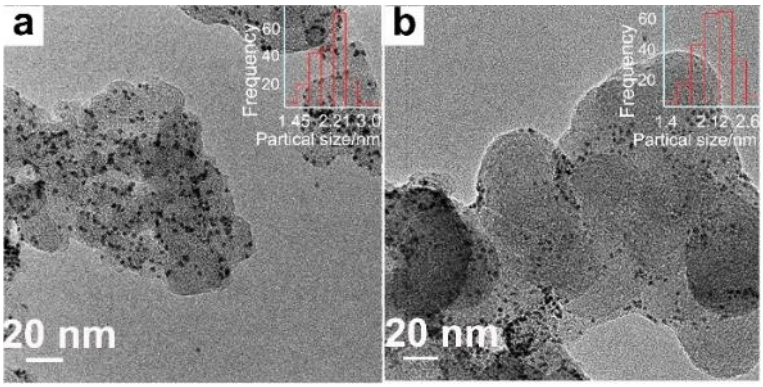

**Figure S6.** Digital photograph (A) of the corresponding supernatants by the washing treatment and HAADF-STEM-EDS mapping images (B) of USCS$^{2h}$ $Au_{38.4}$@$Au_{4.1}Pt_{57.5}$-NP/C catalysts.

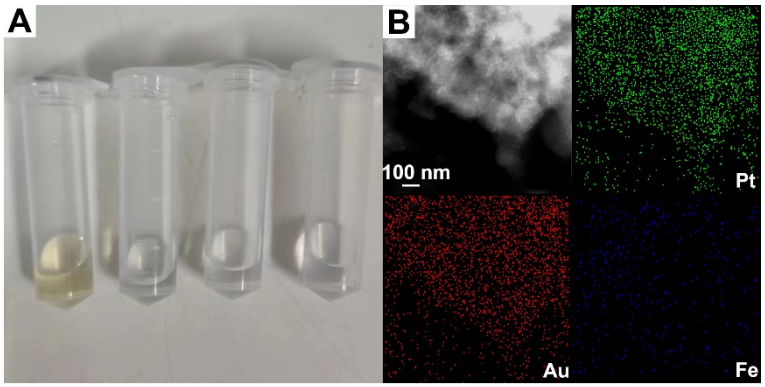


The content of elemental Fe in the USCS$^{2h}$ $Au_{38.4}$@$Au_{4.1}Pt_{57.5}$-NP/C catalysts can be greatly decreased by the washing treatment, which is demonstrated by the variation in the color of the corresponding supernatants (Fig. S6A). As expected, the content of elemental Fe in the USCS$^{2h}$ $Au_{38.4}$@$Au_{4.1}Pt_{57.5}$-NP/C catalysts can be negligible after three cycles of treatments based on the EDS results (Fig. S6B) because only about 3.2 % of elemental Fe in the USCS$^{2h}$ $Au_{38.4}$@$Au_{4.1}Pt_{57.5}$-NP/C catalysts was detected, in compared with those (47.2% and 49.6%) of Au and Pt. The results are also in good agreement with ICP-AES results (42.7% of Au, 55.5% of Pt and 1.8% of Fe).

**Figure S7.** XPS spectra of Pt 4f signals (A) and the Au 4f signals (B) of USCS$^0$ Au@AuPt-NP/C catalysts.

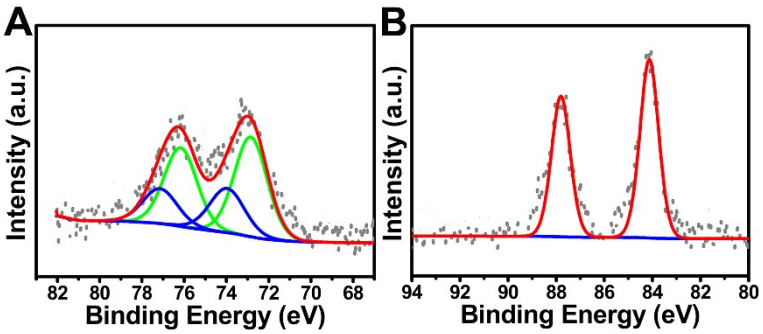

**Figure S8.** CO stripping voltammograms of commercial Pt/C catalysts (A), USCS$^{0}$ Au@AuPt-NP/C catalysts (B) and USCS$^{2h}$ $Au_{38.4}$@$Au_{4.1}Pt_{57.5}$-NP/C catalysts (C). The first and second cycles are displayed as the red lines and black lines, respectively.

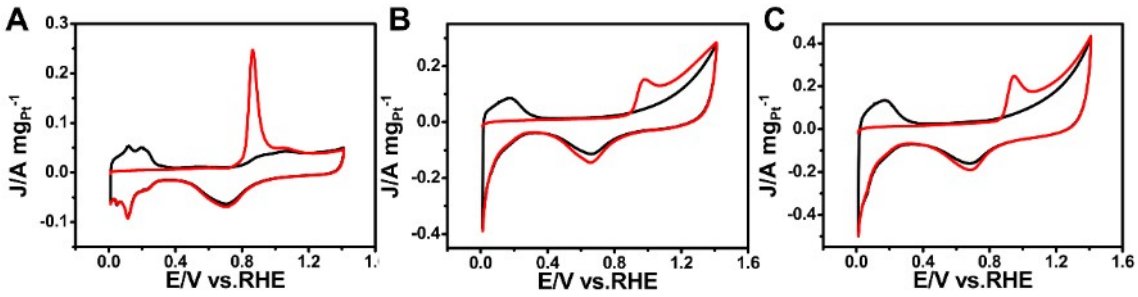

**Figure S9.** TOF curves (A) and histograms (B) of the corresponding TOF values at the overpotential of 0.03 V (vs RHE) of commercial Pt/C catalysts (a), USCS$^{0}$ Au@AuPt-NP/C catalysts (b) and USCS$^{2h}$ $Au_{38.4}$@$Au_{4.1}Pt_{57.5}$-NP/C catalysts (c).

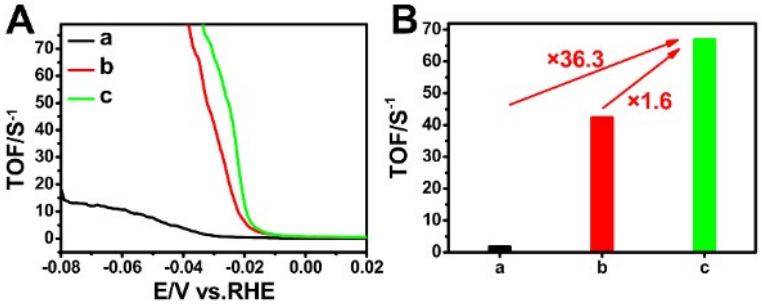

**Figure S10.** TEM images of USCS$^{2h}$ $Au_{38.4}$@$Au_{4.1}Pt_{57.5}$-NP/C catalysts (a, b and c) and commercial Pt/C catalysts (d, e and f) before (a and d) and after the ADT of 10k cycles towards HER (b and e) and ORR (c and f).

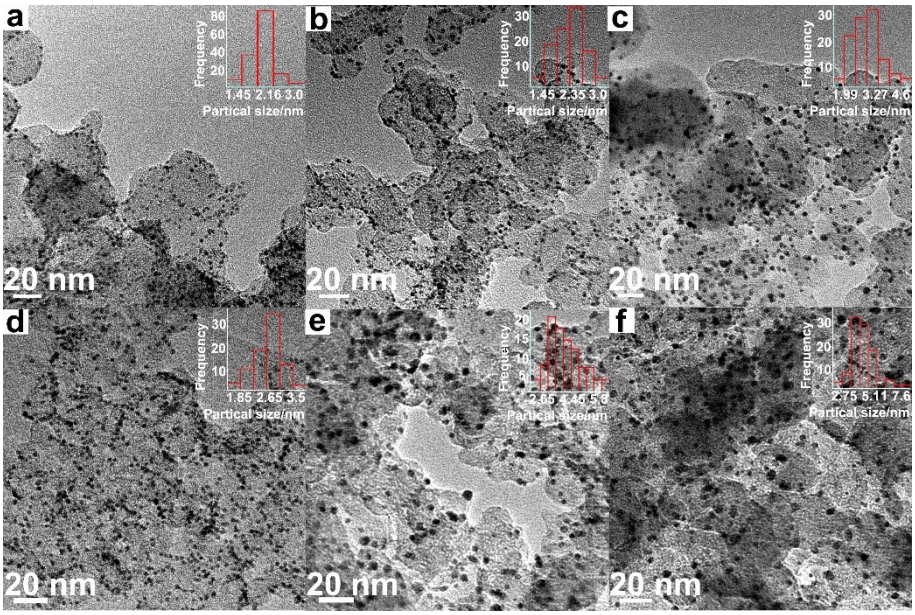

**Fig. S11** CV curves of USCS$^{2h}$ $Au_{38.4}$@$Au_{4.1}Pt_{57.5}$-NP/C catalysts before (black solid curve) and after the ADT of 5k (red dashed curve) and 10k (green dashed curve) cycles towards HER.

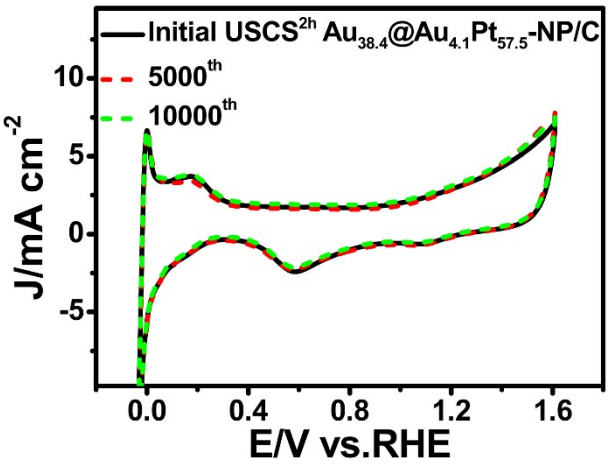

**Figure S12.** LSV curves of commercial Pt/C catalysts (A), USCS$^{0}$ Au@AuPt-NP/C catalysts (B) and USCS$^{2h}$ $Au_{38.4}$@$Au_{4.1}Pt_{57.5}$-NP/C catalysts (C) towards ORR tested at a rotation rate ranging from 400 to 1600 rpm.

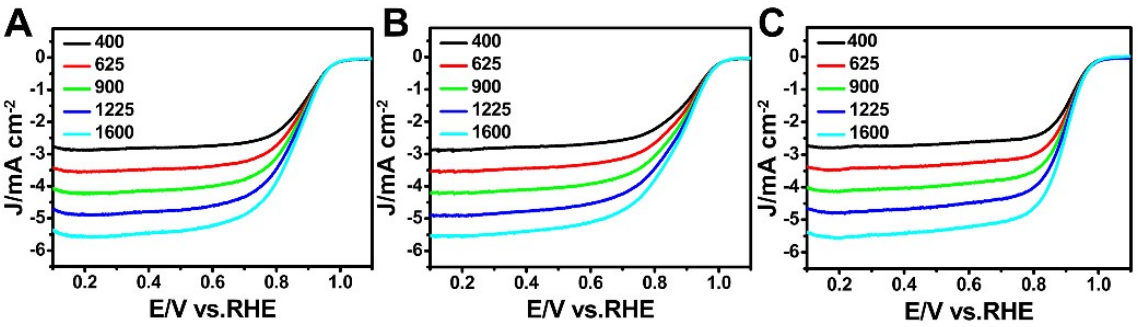

**Figure S13.** Chronoamperometric (CA) curves of commercial Pt/C catalysts (black line) and USCS$^{2h}$ $Au_{38.4}$@$Au_{4.1}Pt_{57.5}$-NP/C catalysts (green line) at 0.5 V (vs. RHE) measured in $O_2$-saturated 0.1 M $HClO_4$ with a rotation speed of 1600 rpm.

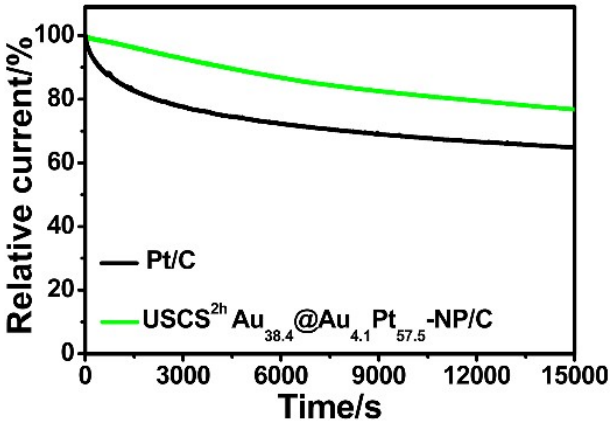

**Figure S14.** CV curves of USCS$^{2h}$ $Au_{38.4}@Au_{4.1}Pt_{57.5}$-NP/C catalysts before (black solid curve) and after the ADT of 5k (red dashed curve) and 10k (green dashed curve) cycles towards ORR.

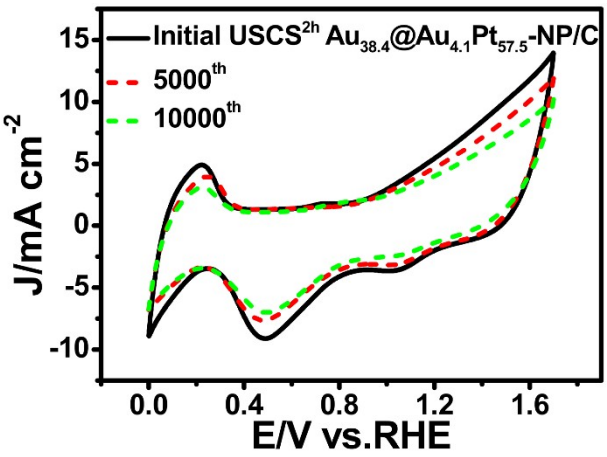

**Table S1.** Summarized data of atomic ratios (at.%) of Au and Pt obtained by CV curves, Pt-to-Au atomic ratios and reduction peak positions of Pt oxide of USCS$^{mh}$ Au@AuPt-NP/C catalysts (a to d) obtained by etching of USCS Au@AuPt-NP/C catalysts in the $FeCl_3$ solution (33 mM, pH = 1.5) under different times: USCS$^{0}$ Au@AuPt-NP/C catalysts (a, 0 h), USCS$^{1h}$ Au@AuPt-NP/C catalysts (b, 1 h), USCS$^{2h}$ Au@AuPt-NP/C catalysts (c, 2 h), and USCS$^{3h}$ Au@AuPt-NP/C catalysts (d, 3 h). The corresponding data of commercial Pt/C catalysts (e) were also shown for comparison.

| Catalysts | Au (at.%) | Pt (at.%) | Pt-to-Au atomic ratio | Reduction peak positions of Pt oxide [V] |
|---|---|---|---|---|
| a | 14.6% | 85.4% | 5.8 | 0.520 |
| b | 9.3% | 90.7% | 9.8 | 0.493 |
| c | 6.7% | 93.3% | 14.0 | 0.488 |
| d | 9.2% | 90.8% | 9.9 | 0.494 |
| e | 0 | 100% | - | 0.64 |

**Table S2.** Summarized data of the total and surface compositions of USCS$^{0}$ Au@AuPt-NP/C catalysts and USCS$^{2h}$ $Au_{38.4}@Au_{4.1}Pt_{57.5}$-NP/C catalysts obtained by ICP-AES and CV curves.

| Catalysts | Total content (at. %) | | Surface content (at. %) | | | |
|---|---|---|---|---|---|---|
| | Au | Pt | Au | Pt | $m_{Au}$ | $m_{Pt}$ |
| USCS$^{0}$ Au@AuPt-NP/C catalysts | 47.7 | 52.3 | 9.3 | 52.3 | 15.1 | 84.9 |
| USCS$^{2h}$ $Au_{38.4}@Au_{4.1}Pt_{57.5}$-NP/C catalysts | 42.5 | 57.5 | 4.1 | 57.5 | 6.7 | 93.3 |

**Table S3.** Summarized data of atomic ratios (at.%) of Au and Pt obtained by EDS, Pt-to-Au atomic ratios and average particle size of USCS$^{mh}$ Au@AuPt-NP/C catalysts (a to d) obtained by etching of USCS Au@AuPt-NP/C catalysts in the $FeCl_3$ solution (33 mM, pH = 1.5) under different times: USCS$^{0}$ Au@AuPt-NP/C catalysts (a, 0 h), USCS$^{1h}$ Au@AuPt-NP/C catalysts (b, 1 h), USCS$^{2h}$ Au@AuPt-NP/C catalysts (c, 2 h), and USCS$^{3h}$ Au@AuPt-NP/C catalysts (d, 3 h).

| Samples | Mean particle size [nm] | Au (at.%) by EDS | Pt (at.%) by EDS | Pt-to-Au (at. %) by EDS |
|---|---|---|---|---|
| a | 2.3±0.5 | 57.1 | 42.9 | 0.75 |
| b | 2.2±0.7 | 54.4 | 45.6 | 0.84 |
| c | 2.2±0.5 | 48.8 | 51.2 | 1.05 |
| d | 2.1±0.9 | 53.4 | 46.6 | 0.87 |

**Table S4.** Summarized binding energies (BEs) of Pt 4f signals of USCS$^{2h}$ $Au_{38.4}$@$Au_{4.1}Pt_{57.5}$-NP/C catalysts and pure Pt NPs.

| Samples | Pt $4f_{5/2}$ peak [eV] | Pt $4f_{7/2}$ peak [eV] | $\Delta$Pt $4f_{7/2}$ peak [eV] |
|---|---|---|---|
| USCS$^{2h}$ $Au_{38.4}$@$Au_{4.1}Pt_{57.5}$-NP/C catalysts | 75.78 | 72.42 | +0.82 |
| Pure Pt NPs | 74.96 | 71.6 | 0 |

**Table S5.** Summarized binding energies (BEs) of Au 4f signals of USCS$^{2h}$ $Au_{38.4}$@$Au_{4.1}Pt_{57.5}$-NP/C catalysts and pure Au NPs.

| Samples | Au $4f_{5/2}$ peak [eV] | Au $4f_{7/2}$ peak [eV] | ΔAu $4f_{7/2}$ peak [eV] |
|---|---|---|---|
| USCS$^{2h}$ $Au_{38.4}$@$Au_{4.1}Pt_{57.5}$-NP/C catalysts | 87.46 | 83.79 | −0.29 |
| Pure Au NPs | 87.75 | 84.08 | 0 |

**Table S6.** Summarized binding energies (BEs) of Au 4f and Pt 4f signals of USCS$^0$ Au@AuPt-NP/C catalysts, pure Au NPs and pure Pt NPs.

| Samples | Au | | | Pt | | |
|---|---|---|---|---|---|---|
| | Au $4f_{5/2}$ peak [eV] | Au $4f_{7/2}$ peak [eV] | ΔAu $4f_{7/2}$ peak [eV] | Pt $4f_{5/2}$ peak [eV] | Pt $4f_{7/2}$ peak [eV] | ΔPt $4f_{7/2}$ peak [eV] |
| USCS$^0$ Au@AuPt-NP/C catalysts | 87.55 | 83.88 | −0.2 | 76.18 | 72.82 | +1.22 |
| Pure Au NPs | 87.75 | 84.08 | 0 | - | - | - |
| Pure Pt NPs | - | - | - | 74.96 | 71.6 | 0 |

**Table S7.** Summarized data of the content of Pt(0) and Pt(II) of USCS$^{2h}$ $Au_{38.4}$@$Au_{4.1}Pt_{57.5}$-NP/C catalysts, USCS$^{0}$ Au@AuPt-NP/C catalysts and pure Pt NPs.

| Samples | Pt(0) | Pt(II) |
|---|---|---|
| USCS$^{2h}$ $Au_{38.4}$@$Au_{4.1}Pt_{57.5}$-NP/C catalysts | 79.07 | 20.93 |
| USCS$^{0}$ Au@AuPt-NP/C catalysts | 74.66 | 25.34 |
| Pure Pt NPs | 58.37 | 41.63 |

**Table S8.** Summarized data of CO stripping voltammograms of commercial Pt/C catalysts, USCS$^{0}$ Au@AuPt-NP/C catalysts and USCS$^{2h}$ $Au_{38.4}@Au_{4.1}Pt_{57.5}$-NP/C catalysts.

| Catalysts | CO stripping peak potential [V] | Onset potential [V] |
|---|---|---|
| Commercial Pt/C catalysts | 0.864 | 0.776 |
| USCS$^{0}$ Au@AuPt-NP/C catalysts | 0.982 | 0.899 |
| USCS$^{2h}$ $Au_{38.4}@Au_{4.1}Pt_{57.5}$-NP/C catalysts | 0.948 | 0.873 |

**Table S9.** Comparison in HER activity in acidic electrolyte of our sample with that of other catalysts reported in literature.

| Catalysts | Overpotential@ 10mA $cm^{-2}$ [mV] | $\Delta\eta_{10}$ vs. Pt/C [mV] | Tafel slop [mV $dec^{-1}$] | Ref. |
|---|---|---|---|---|
| USCS$^{2h}$ $Au_{38.4}@Au_{4.1}Pt_{57.5}$-NP/C | 13 | 18 | 11 | This work |
| Pt SA-PNPM | 35 | negative | 31 | 3 |
| PtCu/$WO_3$@CF | 41 | −10 | 45.9 | 4 |
| $Pt_{0.47}$-Ru/Acet | 28 | negative | 33.3 | 5 |
| $Pt_{(110)}$-$Ni_3N$ | 33 | −6 | 44.9 | 6 |
| Pt/MOF-O | 28 | 15 | 24.4 | 7 |
| Au@$AuIr_2$ | 29 | −3 | 15.6 | 8 |
| Pt–$V_2CT_x$ | 27 | −9.5 | 36.5 | 9 |
| $Mo_2C$@NC@Pt | 27 | −5 | 28 | 10 |
| O-Pt on Au NDs | 18 | 0 | 31 | 11 |
| Pt/CNTs-ECR | 34 | 9 | 26 | 12 |

**Table S10.** Summarized data of the total and surface compositions of USCS$^{2h}$ $Au_{38.4}$@$Au_{4.1}Pt_{57.5}$-NP/C catalysts before and after the ADT of 5k and 10k cycles towards HER, which were obtained by results of ICP-AES and CV curves.

| Catalysts | Total content (at. %) | | Surface content (at. %) | | | |
|---|---|---|---|---|---|---|
| | Au | Pt | Au | Pt | $m_{Au}$ | $m_{Pt}$ |
| USCS$^{2h}$ $Au_{38.4}$@$Au_{4.1}Pt_{57.5}$-NP/C catalysts | 42.5 | 57.5 | 4.1 | 57.5 | 6.7 | 93.3 |
| After 5000 cycles | 42.5 | 57.5 | 4.1 | 57.5 | 6.7 | 93.3 |
| After 10000 cycles | 42.9 | 57.1 | 4.5 | 57.1 | 6.9 | 93.1 |

**Table S11.** Comparison in ORR activity in acidic electrolyte of our sample with that of other catalysts reported in literature.

| Catalysts | ΔE vs. Pt/C [mV] | Mass activity at 0.8 v/0.9 V [$A \cdot mg_{Pt}^{-1}$] | Ref. |
|---|---|---|---|
| USCS$^{2h}$ $Au_{38.4}$@$Au_{4.1}Pt_{57.5}$-NP/C | 38 | 0.88/0.276 | This work |
| $Pt_5Ni_{36}$/CNFs | 30 | - | 13 |
| p-o-PdFe@Pt | 30 | -/0.36 | 14 |
| $Pt_{NP}/Mo_2C$ | 10 | -/0.224 | 15 |
| $Pt_{IL}$-HCNs | - | 0.318/0.135 | 16 |
| Pt/ACMWCNT | 20 | 0.721/0.223 | 17 |
| TKK $Pt_3Co$/C | - | -/0.23 | 18 |
| Pt–Ni@PtD/G | 8 | - | 19 |
| Pt/Vulcan | - | -/0.18 | 20 |
| $Pt_{2.0\ nm}$/Se/C | - | -/0.29 | 21 |
| $Pt_{0.7}Ni_{0.3}$/C | 14 | -/0.283 | 22 |
| Pt NCs(1.4 nm)/OMC | 16 | 0.423/0.198 | 23 |
| $Pt_{71}Co_{29}$ LNFs | - | 0.128(@0.75 V) | 24 |

**Table S12.** Summarized data of the total and surface compositions of USCS$^{2h}$ $Au_{38.4}@Au_{4.1}Pt_{57.5}$-NP/C catalysts before and after the ADT of 5k and 10k cycles towards ORR, which were obtained by results of ICP-AES and CV curves.

| Catalysts | Total content (at. %) | | Surface content (at. %) | | | |
|---|---|---|---|---|---|---|
| | Au | Pt | Au | Pt | $m_{Au}$ | $m_{Pt}$ |
| USCS$^{2h}$ $Au_{38.4}@Au_{4.1}Pt_{57.5}$-NP/C catalysts | 42.5 | 57.5 | 4.1 | 57.5 | 6.7 | 93.3 |
| After 5000 cycles | 43.2 | 56.8 | 4.8 | 56.8 | 7.8 | 92.2 |
| After 10000 cycles | 43.5 | 56.5 | 3.7 | 56.5 | 6.2 | 93.8 |

## References


1 Y. Li, W. Ding, M. Li, H. Xia, D. Wang and X. Tao, *J. Mater. Chem. A*, 2015, **3**, 368-376.

2 H. Xia, Y. Xiahou, P. Zhang, W. Ding and D. Wang, *Langmuir*, 2016, **32**, 5870–5880.

3 W. Peng, J. Han, Y. Lu, M. Luo, T. Chan, M. Peng and Y. Tan, *ACS Nano*, 2022, **16**, 4116-4125.

4 L. Liu, Y. Wang, Y. Zhao, Y. Wang, Z. Zhang, T. Wu, W. Qin, S. Liu, B. Jia, H. Wu, D. Zhang, X. Qu, M. Chhowalla and M. Qin, *Adv. Funct. Mater.*, 2022, **32**, 2112207.

5 Y. Chen, J. Li, N. Wang, Y. Zhou, J. Zheng and W. Chu, *Chem. Eng. J.*, 2022, **448**, 137611.

6 S. Qiao, Q. He, Q. Zhou, Y. Zhou, W. Xu, H. Shou, Y. Cao, S. Chen, X. Wu and L. Song, *Nano Res.*, 2022, **DOI: 10.1007/s12274-022-4654-2**.

7 M. Wang, Y. Xu, C. Peng, S. Chen, Y. Lin, Z. Hu, L. Sun, S. Ding, C. Pao, Q. Shao and X. Huang, *J. Am. Chem. Soc.*, 2021, **143**, 16512-16518.

8 H. Wang, Z. Chen, D. Wu, M. Cao, F. Sun, H. Zhang, H. You, W. Zhuang and R. Cao, *J. Am. Chem. Soc.*, 2021, **143**, 4639-4645.

9 S. Park, Y. Lee, Y. Yoon, S. Y. Park, S. Yim, W. Song, S. Myung, K. Lee, H. Chang, S. S. Lee and K. An, *Appl. Catal. B*, 2022, **304**, 120989.

10 J. Chi, J. Xie, W. Zhang, B. Dong, J. Qin, X. Zhang, J. Lin, Y. Chai and C. Liu, *ACS Appl. Mater. Interfaces*, 2019, **11**, 4047-4056.

11 Y. Lai, S. Li, S. M. G, H. Chang, Y. Huang, Y. Li, Y. Chen, S. B. Patil, S. Chang, P. Chen, C. Chang, Y. Chen, C. Pao, J. Chen, C. Wei, I. K. Lin, H. Chou, C. Su, U. Jeng, T. Kuo, C. Wen and D. Wang, *J. Mater. Chem. A*, 2021, **9**, 22901-22912.

12 X. Bao, Y. Gong, Y. Chen, H. Zhang, Z. Wang, S. Mao, L. Xie, Z. Jiang and Y. Wang, *J. Mater. Chem. A*, 2019, **7**, 15364-15370.

13 X. Liu, X. Wan, X. Tan, H. Yang, Y. Yang, J. Shui and X. Wang, *J. Mater. Chem. A*, 2021, **9**, 21051-21056.

14 M. Gong, T. Shen, Z. Deng, H. Yang, Z. Li, J. Zhang, R. Zhang, Y. Hu, X. Zhao, H. Xin and D. Wang, *Chem. Eng. J.*, 2021, **408**, 127297.

15 L. Zhang, T. Yang, W. Zang, Z. Kou, Y. Ma, M. Waqar, X. Liu, L. Zheng, S. J. Pennycook, Z. Liu, X. J. Loh, L. Shen and J. Wang, *Adv. Sci.*, 2021, **8**, 2101344.

16 Q. Li, S. Song and Y. Wang, *ACS Sustainable Chem. Eng.*, 2021, **9**, 14986-14996.

17 N. Bhuvanendran, S. Ravichandran, K. Peng, Q. Xu, L. Khotseng and H. Su, *Appl. Surf. Sci.*, 2021, **565**, 150511.

18 M. Shen, M. Xie, J. Slack, K. Waldrop, Z. Chen, Z. Lyu, S. Cao, M. Zhao, M. Chi, P. N. Pintauro, R. Cao and Y. Xia, *Nanoscale*, 2020, **12**, 11718-11727.

19 X. Lyu, Y. Jia, X. Mao, D. Li, G. Li, L. Zhuang, X. Wang, D. Yang, Q. Wang, A. Du and X. Yao, *Adv. Mater.*, 2020, **32**, 2003493.

20 I. Jiménez-Morales, F. Haidar, S. Cavaliere, D. Jones and J. Rozière, *ACS Catal.*, 2020, **10**, 10399-10411.

21 H. Cheng, Z. Cao, Z. Chen, M. Zhao, M. Xie, Z. Lyu, Z. Zhu, M. Chi and Y. Xia, *Nano*

*Lett.*, 2019, **19**, 4997-5002.
22 J. Liu, J. Lan, L. Yang, F. Wang and J. Yin, *ACS Sustainable Chem. Eng.*, 2019, **7**, 6541-6549.
23 J. Liu, X. Wu, L. Yang, F. Wang and J. Yin, *Electrochim. Acta*, 2019, **297**, 539-544.
24 L. Zhang, X. Zhang, X. Chen, A. Wang, D. Han, Z. Wang and J. Feng, *J. Colloid Interface Sci.*, 2019, **536**, 556-562.